URSI GASS 2020, Rome, Italy, 29 August - 5 September 2020

Quantification of the artificial mains network impedance contribution to the uncertainty of conducted emission measurements

Carlo F. M. Carobbi
Department of Information Engineering, University of Florence, Firenze, Italy

Abstract

Non-reproducibility of conducted emission measurement due to the deviation from the nominal value of the artificial mains network impedance is here analyzed and quantified. Mean, standard deviation and coverage intervals are derived for the magnitude of the disturbance voltage developed across the input of the receiver. It is demonstrated that the width of the coverage interval depends on the domain spanned by the input quantities to the measurement model, namely the impedance of the artificial mains network and the impedance of the equipment under test. Different degrees of severity, determining a narrower or wider coverage interval but always corresponding to a coverage probability of 95 %, are identified.

1 Introduction

The non-reproducibility and uncertainty of electromagnetic compatibility (EMC) measurements is a topic of investigation triggered by the needs of both standards' improvement and compliance of testing laboratories to the requirements of ISO/IEC 17025 [1] (namely, measurement uncertainty quantification and participation to interlaboratory comparisons). Several studies were devoted to the non-reproducibility and uncertainty of radiated emission measurements [2-4], conducted emission measurements [5-8], radiated immunity [9, 10] and conducted immunity to impulses [11, 12].

The non-reproducibility of conducted emission measurement due to the imperfection (i.e. deviation from nominal) of the artificial mains network (AMN) impedance has been recently investigated by several authors in order to quantify the interval of the possible values of the disturbance voltage [4, 5, 6]. Such non-reproducibility is the dominating contribution to measurement uncertainty of conducted disturbances [13]. An original analysis is here offered, based on the theoretical approach described in [6], in order to derive coverage intervals for the disturbance voltage corresponding to different assumptions on the domain spanned by the input to the measurement model, namely the actual impedance of the AMN and the impedance of the equipment under test (EUT). The mathematical analysis is carried out in section 2, while the numerical application is developed in section 3. Conclusion follows in section 4.

2 Analysis

The problem is described by using the equivalent circuit in Figure 1, where U_{d0} is the open-circuit disturbance voltage generated by the EUT, Z_{d0} is the EUT impedance, Z_{13} is the nominal AMN impedance, as defined by the standards specification, and Z_{in} is the actual impedance. Since Z_{in} shall unavoidably differ from Z_{13}, also the voltage developed across these impedances by the same EUT, U_m and U_{mt}, respectively, will be different. The measurement non-reproducibility is quantified through the relative deviation δ between U_m and U_{mt}, namely

$$\delta = \frac{U_m - U_{mt}}{U_{mt}} . \tag{1}$$

The impedance of the EUT, Z_{d0}, is an unspecified parameter. Its value and frequency behavior depend on the specific EUT and they are usually unknown. It is assumed that Z_{d0} can be any complex value in the right half of the complex impedance including the imaginary axis.

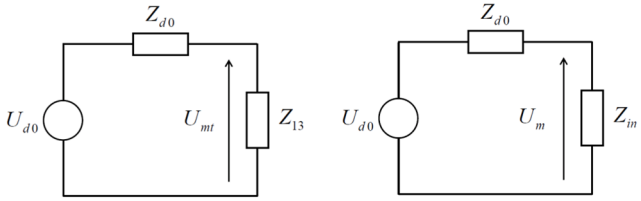

Figure 1. Circuit description of the problem of measurement non-reproducibility due to the imperfection of the AMN impedance: (left) measurement with an ideal AMN, (right) measurement with a real AMN.

The concept of the "impedance tolerance circle", as defined in [14], is also adopted here. According to this concept Z_{in} shall be such that

$$\frac{Z_{in}}{Z_{13}} = 1 + z, \tag{2}$$

where $z = \rho e^{j\theta}$ and ρ is a real value within the interval $[0, \rho_M]$ and θ shall be within $[0, 2\pi)$. Through the concept of the impedance tolerance circle constraints on the magnitude and phase of Z_{in} are then derived as

$$1 - \rho_M \le \frac{|Z_{in}|}{|Z_{13}|} \le 1 + \rho_M \tag{3}$$

and

$$-\arcsin\left(\rho_M\right) \le \arg\left(\frac{Z_{in}}{Z_{13}}\right) \le \arcsin\left(\rho_M\right). \qquad (4)$$

In [14] $\rho_M = 0.2$. Note that if Z_{in} is within the impedance tolerance circle then (3) and (4) are met. Contrarily, if Z_{in} meets (3) and (4) then Z_{in} may get values outside the impedance tolerance circle. AMN compliance with CISPR requirements is assessed through (3) and (4). Now note that

$$1+\delta = \frac{U_m}{U_{mt}} = \frac{1+z}{1+zk}, \qquad (5)$$

where

$$k = \frac{Z_{13}}{Z_{d0}+Z_{13}} \qquad (6)$$

represents the voltage division ratio between the EUT impedance and the ideal AMN impedance. k, together with z, concurs to determine the magnitude of the deviation between U_m and U_{mt} which quantifies the non-reproducibility. The domain of z, D_z, is a disc in the complex plane centered at the origin and with radius ρ_M, see (2). Similarly, the transformation (6), as it is demonstrated in [6], maps the right half of the complex plane of Z_{d0} into a disc of the complex plane of k. Such disc (domain D_k) is centered at k_O and has a radius $|k_O|$ where

$$k_O = \frac{1}{2}\left(1 + j\frac{X_{13}}{R_{13}}\right), \qquad (7)$$

$R_{13} = \mathrm{Re}\left(Z_{13}\right)$ and $X_{13} = \mathrm{Im}\left(Z_{13}\right)$. The transformation from the complex plane of Z_{d0} to that of k is represented in Figure 2, where $k_M = 2k_O$.

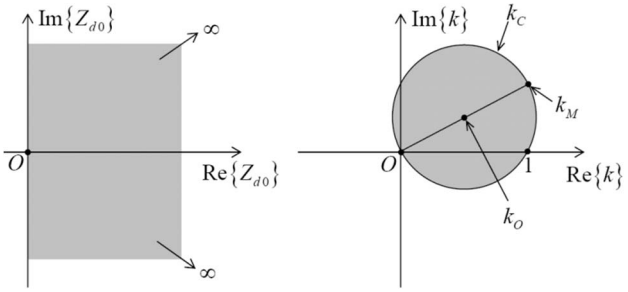

Figure 2. The domain of Z_{d0}, gray area on the left side, and the corresponding domain of k, gray area (disc) on the right side.

The imaginary axis of the complex plane of Z_{d0} is transformed into the perimeter k_C of the disc in the complex plane of k. Further, while the domain of Z_{d0} has infinite size that of k has finite size, thus simplifying the numerical derivations detailed in the following section.

3 Application

In order to evaluate the measurement non-reproducibility random sampling is carried out over the domains of z and k thus generating random samples of the non-reproducibility, as quantified by

$$20\log_{10}\left(|1+\delta|\right) = 20\log_{10}\left(\left|\frac{1+z}{1+zk}\right|\right). \qquad (8)$$

Logarithmic units are used since non-reproducibility is usually expressed in decibels. We are interested in the coverage interval of the possible values of $20\log_{10}\left(|1+\delta|\right)$ corresponding to a coverage probability of 95 %.

We consider the case of the 50 Ω||(50 µH + 5 Ω) AMN [14], the network designed to cover the broad frequency range from 9 kHz to 30 MHz and adopted by many product standards.

Note that the magnitude of the denominator of (5) is greater than 0 if $\rho_M|k_M| < 1$ and this inequality is met by the impedance of the 50 Ω||(50 µH + 5 Ω) AMN over the whole frequency range of operation. As a consequence (5) is an analytic function of z and k over the limited size regions D_z and D_k. Due to the properties of analytic functions the maximum (limited) and minimum (greater than 0) magnitudes of (5) exist and they are achieved on the borders of such regions. This property of the magnitude of (5) suggests different options for randomly (Monte Carlo, [15]) sampling the domains D_z and D_k and thus obtaining different ranges of the coverage interval. In particular, the smaller range (smaller variability) is expected when randomly sampling the interior of D_z and D_k while the larger one (larger variability) is expected when sampling the borders of D_z and D_k.

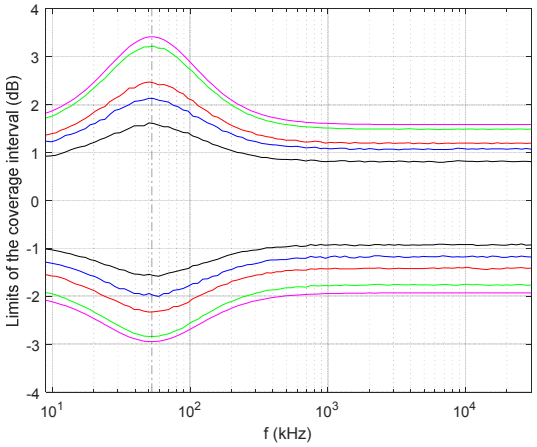

Figure 3. Minimum and maximum limits of the 95 % coverage interval as a function of frequency.

The results of Monte Carlo sampling are illustrated in Figure 3, where the limits of the 95 % probabilistically symmetric coverage interval are plotted, and in Figure 4, showing the range of the 95 % coverage interval (difference between the maximum and the minimum limits), both as a function of frequency. Different colors correspond to different sampling strategies. The black lines result from uniformly sampling the interior of the domains

of D_z and D_k. Uniform sampling over both discs is obtained through uniform sampling of the radius (from 0 to ρ_M and from 0 to $|k_O|$) and of the angle around the center of the disc (from 0 to 2π). The blue lines result from uniform sampling of k over the border of the disc D_k (imaginary EUT impedance) while z is uniformly sampled over the interior of the disc D_z. The red lines result from uniform sampling of z over the border of the disc D_z (AMN impedance at the tolerance limit) and of k over the interior of the disc D_k. The green lines result from uniform sampling of both the borders of the discs D_z and D_k. Finally, the magenta lines result from uniform sampling over the border of the disc D_z and from setting $k = \hat{k} = \dfrac{1}{\rho_M^2 - j\dfrac{R_{13}}{X_{13}}}$. $\hat{k}$ is a value on the border of D_k and such that the root-mean-square value of the magnitude of (5), for z varying over the border of D_z, is maximum [6]. $k = \hat{k}$ corresponds to the worst case EUT impedance $Z_{d0} = -j\dfrac{|Z_{13}|^2\left(1-\rho_M^2\right)}{X_{13}}$.

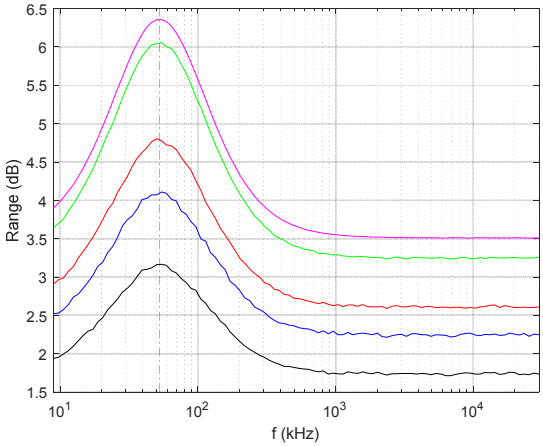

Figure 4. Range of the 95 % coverage interval as a function of frequency.

Note that the maximum range of the coverage interval is obtained at the frequency of 52,8 kHz where the maximum phase angle of the impedance of the 50 Ω||(50 µH + 5 Ω) AMN is achieved.

In [13] the limits of error due to the 50 Ω||(50 µH + 5 Ω) AMN impedance are −3.6 dB (lower) and +3.1 dB (upper) and a triangular distribution is assumed centered at 0 dB and having a standard deviation of 1.37 dB. In order to compare [13] with the results here reported the standard uncertainty and the mean corresponding to each sampling strategy are plotted in Figure 5 and in Figure 6, respectively, as a function of frequency. It is confirmed that the mean is practically zero for all the sampling strategies and over the full frequency range. The triangular probability density function approximates the probability density functions that are numerically derived in this study.

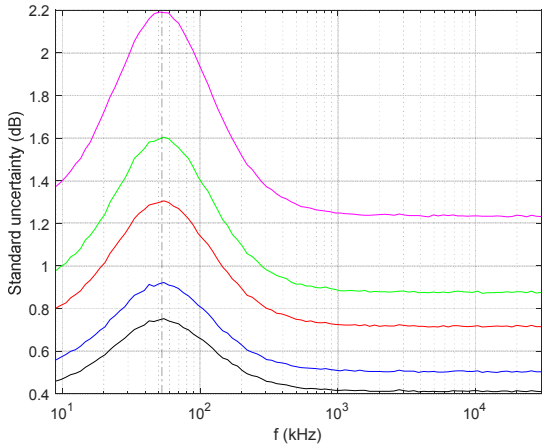

Figure 5. Standard uncertainty as a function of frequency.

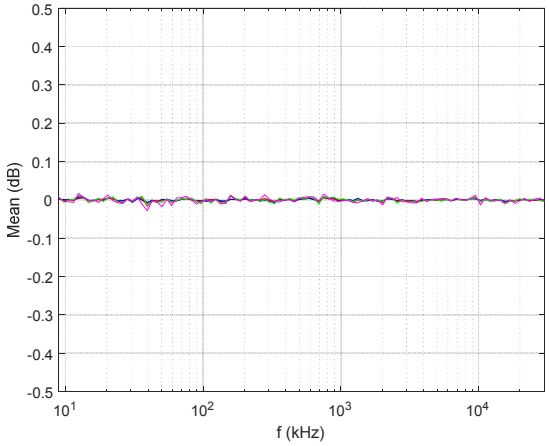

Figure 6. Mean as a function of frequency.

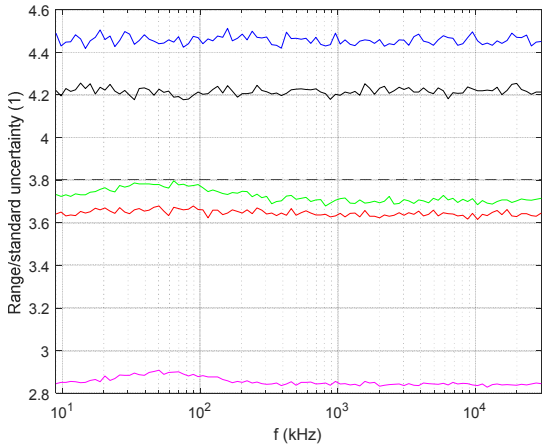

Figure 7. Ratio of the range (corresponding to 95 % coverage probability) over the standard uncertainty, as a function of frequency. Dashed line represents the same ratio assuming a triangular probability density function.

The ratio between the range and the standard uncertainty is shown in Figure 7. In the case of the triangular distribution the value of this ratio is $2\sqrt{6}\left(1-\sqrt{0.05}\right) \approx 3.8$ and it is represented through a dashed line in Figure 7. The

triangular distribution appears suitable to describe the spread of the possible values in the case represented by the green curve, namely when both z and k uniformly sample the borders of the corresponding domains, D_z and D_k.

4 Conclusion

The non-reproducibility of the disturbance voltage due to the imperfect realization of the AMN impedance is a knowledge-based source of uncertainty, i.e. not based on experimental observation. Experimental observation would require experiments involving EUTs characterized by all the possible disturbance source impedances and AMNs characterized by all the possible deviations from the nominal impedance, which is clearly impossible. According to the experience of the author, AMN impedance is close to the tolerance limits at the lowest and highest frequencies. Further, the impedance of the disturbance source is dominated by the output impedance of the filter used to attenuate disturbances at the power port, which is essentially reactive. Hence it is safe but also reasonable to estimate the non-reproducibility assuming that z and k are at the borders of their respective domains D_z and D_k (results corresponding to the green curves in the plots from Figure 3 to Figure 7). Similarly to the case of the mismatch correction [16], the expected value of the non-reproducibility is zero.

7 References

1. ISO/IEC 17025:2017, "General requirements for the competence of testing and calibration laboratories."

2. C. F. M. Carobbi, M. Cati, C. Panconi, "Reproducibility of Radiated Emissions Measurements in Compact, Fully–Anechoic, Rooms — The Contribution of the Site-to-Site Variations," IEEE Transactions on Electromagnetic Compatibility, vol. 51, no. 3, pp. 574-582, Aug. 2009.

3. C. F. M. Carobbi, A. Bonci, M. Cati, C. Panconi, M. Borsero and G. Vizio, "Design, Preparation, Conduct and Result of a Proficiency Test of Radiated Emission Measurements", IEEE Transactions on Electromagnetic Compatibility, vol. 56, no. 6, pp. 1251-1261, Dec. 2014.

4. C. F. M. Carobbi, A. Bonci, M. Cati, C. Panconi, M. Borsero and G. Vizio, "Proficiency Testing by Using Traveling Samples With Preassigned Reference Values", IEEE Transactions on Electromagnetic Compatibility, vol. 58, no. 4, pp. 1339 – 1348, Aug. 2016.

5. M. Stecher, "Uncertainty in RF Disturbance Measurements: Revision of CISPR 16-4-2," Proceedings of the IEEE International Symposium on Electromagnetic Compatibility, Kyoto, 2009.

6. C. F. M. Carobbi and M. Stecher, "The Effect of the Imperfect Realization of the Artificial Mains Network Impedance on the Reproducibility of Conducted Emission Measurements," IEEE Transactions on Electromagnetic Compatibility, vol. 54, no. 5, pp. 986-997, Oct. 2012.

7. A. Kriz, "Uncertainty calculation for AMN impedance contribution using the Monte Carlo Method," 2019 IEEE Int. Symp. on EMC, New Orleans (LO), Jul. 22-36, 2019, pp. 565-569.

8. C. Carobbi, "Reproducibility of Conducted Disturbance Measurements," IEEE 17th International Conference on Environment and Electrical Engineering, Milano (Italy), June 6-9, 2017.

9. C. F. M. Carobbi, "The Statistical Field Uniformity Criterion in Transverse Electromagnetic Waveguides," IEEE Transactions on Electromagnetic Compatibility, vol. 59, no. 6, pp. 2052 – 2053, Dec. 2017.

10. C. F.M. Carobbi, G. Borio, D. Festa, A. Zanobini, "Field non-uniformity over the uniform field area as per IEC 61000-4-3 radiated immunity test", IMEKO TC4 Int. Symp., Kosice, Slovakia, Sep. 8-10, 2010.

11. C. F. M. Carobbi, A. Bonci, M. Stellini, M. Borsero, "Time-Domain Characterization of the Surge, EFT/Burst and ESD Measurement Systems," IEEE Transactions on Instrumentation and Measurement, vol. 62, no. 6, pp. 1840-1846, Jun. 2013.

12. C. F. M. Carobbi, "Measurement Error of the Standard Unidirectional Impulse Waveforms Due to the Limited Bandwidth of the Measuring System," IEEE Transactions on Electromagnetic Compatibility, vol. 55, no. 4, pp. 692-698, Aug. 2013.

13. Specification for radio disturbance and immunity measuring apparatus and methods – Part 4-2: Uncertainties, statistics and limit modeling – Uncertainty in EMC measurements, CISPR 16-4-2:2011+AMD 1:2014+AMD 2:2018.

14. Specification for radio disturbance and immunity measuring apparatus and methods – Part 1-2: Radio disturbance and immunity measuring apparatus – Ancillary equipment – Conducted disturbances, CISPR 16-1-2:2014+AMD 1:2017.

15. BIPM, IEC, IFCC, ILAC, ISO, IUPAC, IUPAP and OIML, 2008 Supplement 1 to the 'Guide to the Expression of Uncertainty in Measurement'—Propagation of distributions using a Monte Carlo method JCGM 101:2008 www.bipm.org/utils/common/documents/jcgm/JCGM 101 2008 E.pdf

16. C. F. M. Carobbi, M. Cati, C. Panconi, "Note on the Expected Value and Standard Deviation of the Mismatch Correction," IEEE Transactions on Electromagnetic Compatibility, vol. 53, no. 4, pp. 1098-1099, Nov. 2011.